Available online at www.sciencedirect.com

SciVerse ScienceDirect

Energy Procedia 37 (2013) 3621 – 3629

Energy Procedia

GHGT-11

Multi-phase equilibrium in a CO_2-filled observation well at the Ketzin pilot site

Matteo Loizzo[a,*], Jan Henninges[b], Martin Zimmer[b], and Axel Liebscher[b]

[a]*Schlumberger Carbon Services; now wellbore integrity consultant, Helmstedter Str. 21, 10717 Berlin, Germany*
[b]*GFZ German Research Centre for Geosciences, Telegrafenberg, 14473 Potsdam, Germany*

Abstract

As part of the Ketzin pilot test site, carbon dioxide (CO_2) has been injected into a saline formation around 650 m deep since June 2008. Analysis of measured well temperature and pressure data at two observation wells after the arrival of CO_2 has shown that two-phase fluid conditions are prevailing in the upper 400 m of the wells. This significantly hampers the ability to accurately describe the density – and temperature – profile of a well, which is essential to predict the relationship between well-head and reservoir pressure. The pressure and temperature profile depends crucially on the depth of the liquid CO_2 free surface, which can be obtained by wrapping a radial temperature simulator in an optimization algorithm that imposes closure of the heat transport at the well scale. Vertical heat transport, necessary for balancing the heat in- and outflow, relies on the upward movement of CO_2 vapor bubbles in the liquid-dominated zone and by a descending liquid CO_2 film in the upper vapor-dominated zone. A vertical bubble velocity of around 45 mm/s was derived from heat balance and confirmed by camera inspection movie. Temperature and pressure profiles also showed that Ktzi 200 acted as a distillation column: the injected CO_2 (with purity >99.9%), picked up water during the residence in the storage horizon. The extremely accurate equation of state for CO_2 can accurately predict fluid properties in the two-phase zone and reveals that both light and heavy components in the gas entering the well are not present in the two-phase zone. This, together with an analysis of the thermodynamic behavior of the gas mixture suggests that a distillation process purified CO_2, at least in the upper part of the well.

Selection and/or peer-review under responsibility of GHGT

Keywords: pressure, heat transport, thermodynamics, convection, distillation, multi-phase

* Corresponding author. Tel.: +49-176-5732-5545.
E-mail address: matteo.loizzo@mac.com

1876-6102
Selection and/or peer-review under responsibility of GHGT
doi:10.1016/j.egypro.2013.06.255

1. Introduction

1.1. The Ketzin project

Ketzin, in the state of Brandenburg (Germany) is the first European on-shore pilot test site for geological storage of CO_2 in a saline aquifer. The site has been in operation since 2008 Jun 30 and has been managed initially under the CO2SINK and currently under the CO2MAN project [1]. One injection well and two observation wells were drilled to a depth of around 800 m in 2007 [2]. The observation well Ktzi 200, the subject of this paper, is located 50 m from the injector, Ktzi 201. The reservoir horizons are sandstone layers of the Triassic Stuttgart Formation at about 600 to 700 m depth.

The initial reservoir conditions were 33.5°C and 6.1 MPa at a depth of 630 m. After CO_2 arrived at Ktzi 200 in July 2008 [3] wellhead pressure increased and quickly stabilized at a value around 5.1 MPa, remaining constant during the subsequent period of continuous injection, which lasted several months.

Temperature profiles measured with a fiber-optics Distributed Temperature Sensor (DTS) outside of the production casing also reached a stable equilibrium, markedly different from the original geothermal profile [4]. The heat and mass transport phenomena that determined this steady-state condition will be described in this paper. Subsequent changes in injection rate have led to evolutions in the wellhead pressures, and temperature profiles, of both observation wells, with a new steady-state quickly reached after each change; the stability of dynamic equilibrium conditions under different reservoir pressures and temperatures confirmed the validity of the model described below.

Aside from the frequent monitoring of temperature profile through the DTS fiber, repeated wireline pressure and temperature logs were run using the Schlumberger Platform Basic Measurement Sonde (PBMS). Within the current study, a baseline run of Ktzi 200 recorded in June 2008 before start of CO_2 injection when the well was full of reservoir brine, and a repeat run recorded in June 2009, after the well had filled with CO_2 and the new equilibrium established itself, are analyzed. Later, in October 2009 a camera inspection was also run in the monitoring well.

1.2. Fluids and phases

The law of conservation of momentum (i.e. mechanical equilibrium) in the absence of motion reduces to:

$$\frac{dp}{dz} = \rho(p,T)\cdot g \qquad (1)$$

Based on this relationship, the density of the fluid inside the well has been calculated from the measured pressure gradient for the purpose of this study.

The density profile in Fig. 1(a), after Ktzi 200 had filled up with CO_2, allows the identification of four zones, from top to bottom: 1) low density vapor-dominant CO_2 down to 292 m, the liquid CO_2 free surface; 2) liquid-dominant CO_2 down to the critical point around 560 m; 3) a supercritical region down to the brine free surface, at 650 m (the top of the permeable Stuttgart formation); and 4) the reservoir brine down to the bottom of the well (see also [4]).

Pressure and temperature approach the critical point at around 560 m depth: the critical temperature of 31.0°C is reached at 565.9 m and the critical pressure of 7.38 MPa at 557.6 m. Proximity to the critical point causes large variations in density (the isothermal compressibility diverges at the point) as well as what is referred to as “critical enhancement” to transport properties – i.e. viscosity and thermal diffusivity.

Fig. 1(b) shows that the temperature and pressure in Ktzi 200 follow the liquid-vapor saturation curve from the critical point up; the difference between the original geothermal temperature profile and the one recorded after CO_2 filled the well (Fig. 1(a)) implies that heat exchange is taking place above ~400 m, suggesting that above this depth the CO_2 is diphasic: vapor CO_2 bubbles in the liquid-dominant zone and droplets in the vapor-dominant one.

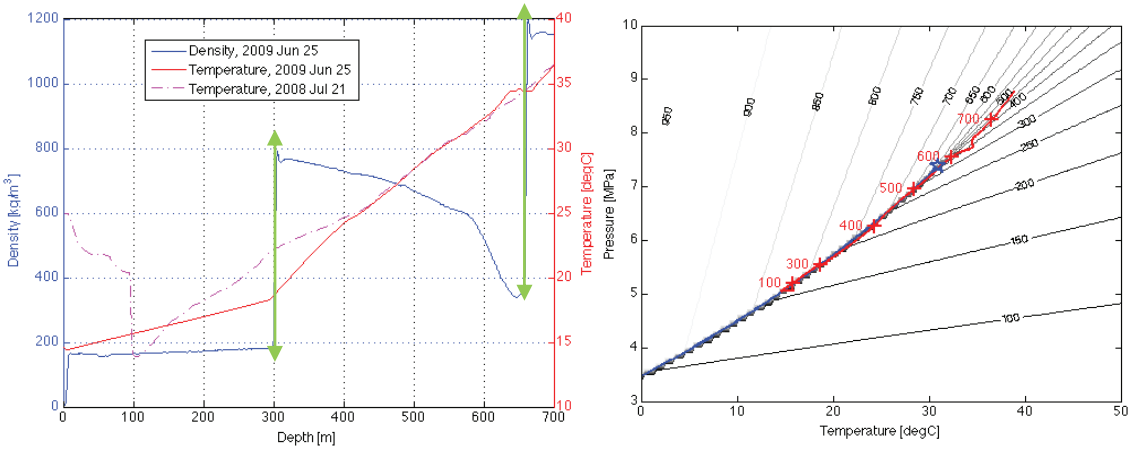

Fig. 1. (a) Temperature profiles in Ktzi 200 measured during the wireline logs before and after CO_2 arrival; the CO_2 density profile, plotted against the left axis, shows the extent of the vapor-dominant zone, the liquid-dominant zone, and the original brine, separated by green vertical lines. (b) Pressure vs. temperature in Ktzi 200 after CO_2 arrival (depth indicated by red crosses) superimposed to the phase diagram of pure CO_2. The vapor-liquid saturation curve is plotted in blue and a star marks the critical point; iso-density curves in the range 100-950 kg/m^3 (spaced by 50 kg/m^3) are also added for reference.

2. Heat transport in Ktzi 200

Higher up the well, vapor condenses against the cooler casing wall and a film of liquid CO_2 flows down the pipe, with some of it evaporating again as it encounters warmer temperatures at greater depths. Evaporation in the saturated liquid section of the well causes inward heat flow (i.e. cooling of the formation) and condensation in the saturated vapor section causes outward heat flow (i.e. heating of the formation), with vertical heat flow provided by the lighter vapor bubbles and the liquid film traveling in opposite direction.

At each point along the saturation line temperature is uniquely determined by pressure, yet density can vary between the values of saturated liquid and vapor depending on the enthalpy (or, equivalently, entropy) of the fluid. Crucially, this “intermediate” fluid is a two-phase mixture of liquid and vapor end-members: its density can only be achieved by having vapor bubbles suspended in the saturated liquid (or droplets in saturated vapor). However as mentioned above, only single-phase fluids – liquid or vapor – are gravitationally stable. A constant mixture at a given depth thus requires continuous generation of bubbles to replace the ones that float upward. Fig. 2 shows the occurrence of such stable mixtures in Ktzi 200: in the saturated liquid part of the well down to 400 m, density is lower than the saturated liquid value; density decreasing towards the liquid CO_2 free surface correspond increasing volume fractions of bubbles; similarly, slightly higher densities measured in the saturated vapor section are due to a mixture with liquid CO_2 (physically, by the tiny drag caused on vapor CO_2 by the liquid film descending along the casing wall).

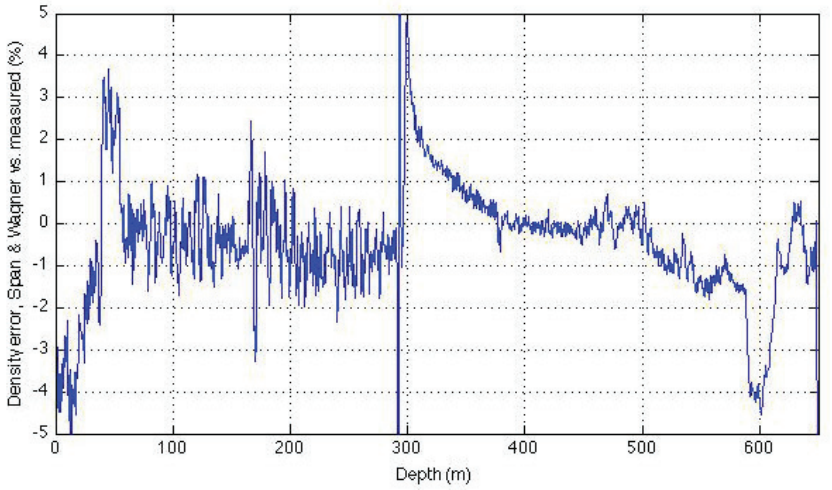

Fig. 2. Predicted density from [6] vs. measured density in Ktzi 200 during the June 2009 wireline logging run. Positive errors means a lighter fluid than pure CO_2 was encountered in the well. In the biphasic region the saturated phase densities were used as reference: above 292 m the saturated vapor density and from 292 to 400 m the saturated liquid density.

3. Prediction of the liquid CO_2 free surface

A key question in properly understanding the diphasic region captured by the saturation curve concerns the position of the liquid CO_2 free surface. Along the saturation curve, if density effects due to vapor-liquid mixtures are neglected, pressure is a function of temperature only; pressure in turn is a function of density (Eq. 1), so in principle one value of pressure, either at the well-head or at the bottom of the diphasic region, is sufficient to determine the whole temperature and pressure profile. In reality, an additional degree of freedom is provided by the depth of the vapor-liquid interface, i.e. the liquid CO_2 free surface.

Below the interface the temperature (thus the pressure) gradient follows the saturated liquid CO_2 density whereas above the interface the saturated vapor density causes a much less steep temperature profile, as displayed in Fig. 3(a). As mentioned above, this picture is only approximate: the density of the two-phase mixture can take any value between saturated vapor and saturated liquid, depending on the enthalpy of the mixture (which in turn is determined by the heat exchange with the environment at each depth). In practice, the maximum observed deviation from the saturated densities is 5% (see Fig. 2), so the CO_2 column can be considered as single-phase saturated vapor overlying saturated liquid.

Like temperature, pressure also display a steeper gradient across the saturated liquid zone so shallower free surfaces result in lower wellhead pressures as more of the bottom-hole pressure is “consumed” by the hydrostatic head of the liquid.

Of course the difference between the formation geothermal profile and the temperature profile in the well, imposed by the saturation line, must involve continuous heat exchange. Constant temperature profiles (at least during phases of constant reservoir pressure) imply that the overall heat balance must be zero, as in a heat pipe: the heat gained by the evaporation of liquid CO_2 at the bottom of the diphasic region must equal the heat released by the condensation of vapor CO_2 at the top. Strictly speaking, the total heat balance can only be zero for a reversible process, i.e. when no friction losses occur; however, given the low viscosity of CO_2, approximate reversibility can be safely assumed in practice.

The only degree of freedom of the diphasic system is the free surface position, which yields a family of temperature profiles, and thus of heat flow distributions: the condition of zero heat flow will thus determine the only possible position of the vapor-liquid interface.

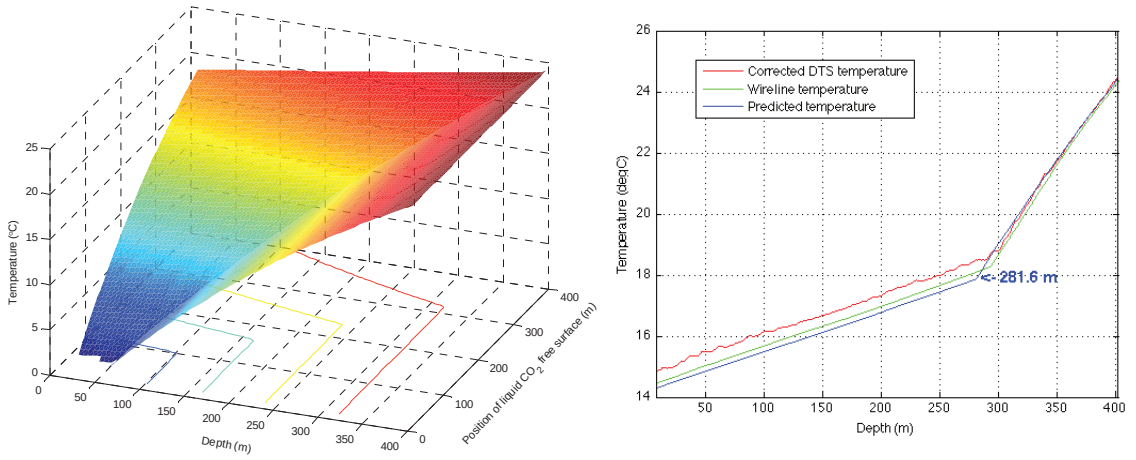

Fig. 3. (a) Temperature profile vs. depth and position of the liquid-vapor boundary; (b) measured temperature profiles over the two-phase section compared to the temperature predicted imposing the zero heat flux condition together with the depth of intersection between hydrostatic pressure and the saturation pressure curve at the bottom of the well.

The free surface depth is obtained by applying an optimization algorithm, with the zero heat flow as a goal, to a series of 1-D radial heat exchange models for casing, cement and formation. Dirichlet boundary conditions are imposed on temperature: at the inner casing radius it must be equal to the value computed from the saturation line (with the imposed free surface depth), and at infinity it must be equal to the undisturbed geothermal profile. The algorithm predicts a free surface depth of 281.6 m, very close to 292 m, the value found by analyzing the logs (Fig. 3(b)). The predicted pressure at 8 m depth is 5.0 MPa, compared with 5.07 MPa measured by wireline (1.4% error). For this simulation, pressure at the capture depth was imposed, in order to better assess the algorithm performance; the capture depth can however also be easily calculated by integrating Eq. 1 upwards from the reservoir.

The condition of zero heat flux is very robust, since it involves an integral over depth, and is fairly insensitive to the detailed thermal diffusivity at each depth. Even the slight departures from the saturated end member densities due to multi-phase conditions don't play a significant role: considering the effect of vapor bubbles on the liquid CO_2 density moves up the free surface depth by less than 1 m.

Of course, this simple model cannot reproduce the complexity of the initial transient while the well is being filled with CO_2, the original brine is siphoned back into the formation and the heat pipe is started. DTS observations however suggest that in Ktzi 200 this transient was of limited duration, and that a pseudo-steady state was fully developed by March 2009. It is worth mentioning that a true steady state cannot be reached in radial heat exchange problems; in reality the free surface reaches a minimum and then moves up again, albeit very slowly and as a function of the logarithm of time: the model predicts that in the 100 days before the log, the free surface had migrated upward by about 1 m.

The zero heat flow condition, while introducing a closing relation to the problem of determining the liquid CO_2 surface, underlines the complexity of relating well-head and bottom-hole pressure for a static column of CO_2. In spite of the difficulties, the task of relating the two pressures is of practical importance: in many cases bottom-hole pressure is not monitored, but deduced from the pressure recorded

at surface; in other cases, e.g. during well design, the prediction of surface pressure in a CO_2 monitoring well is used to safely dimension well-head equipment.

The routine approach is to consider the geothermal temperature profile as fixed and to integrate the mechanical equilibrium equation to the depth of interest, using either the bottom-hole or the well-head pressure as starting point. In many cases the geothermal gradient is crudely approximated by considering a straight line from a reference temperature at surface to the (often measured) bottom-hole temperature. With CO_2 this method will produce unacceptable errors and the algorithm described above should be used instead.

Integrating downwards, i.e. determining the reservoir pressure from the wellhead pressure, relies on a similar, if slightly more complicated, method: for a given free surface depth, CO_2 will follow the saturation line to the depth where the line meets the geothermal profile. An optimization loop must then apply the zero heat flow condition to jointly obtain the free surface and the depth at which hydrostatic pressure departs from the saturation pressure. Afterwards, integration to obtain the bottom-hole pressure is easy.

4. Vapor bubbles vertical velocity

From the difference between the density of saturated liquid CO_2 and the measured one a volume fraction of vapor bubbles (hold-up) can be easily computed, resulting in a roughly linear increase in bubble loading above 400 m with a divergence near the top of the liquid and values <5% everywhere.

The increase in the total mass of bubbles at each depth (related to the vapor hold-up by its density) depends on the heat flowing inward from the casing at that depth. The equation of conservation of mass for vapor is simple to write, yielding a direct relation between the heat flow q, the observed bubble volume fraction Φ and the average vertical velocity of the bubbles w:

$$\mathrm{div}(\rho w \Phi) = \frac{q}{A \Delta h_{ev}} \rightarrow w = \frac{1}{\rho \Phi} \int_{z_0}^{z} \frac{q}{A \Delta h_{ev}} d\zeta \qquad (2)$$

Where A is the specific inner surface area of the casing (0.38 m^2/m), Δh_{ev} is the specific enthalpy of evaporation of CO_2 and z_0 is a suitable depth with no observable bubbles (400 m in this case). The distribution of velocity among all bubbles at a given depth will depend on their size distribution, which is likely to be narrow due to a similar formation mechanism and the negligible change in mass during travel.

The heat flow, q, can be computed using the same 1-D model described in section 3, except that temperature at the casing inner radius is fixed to the value measured during the wireline log 192 days after the arrival of CO_2.

The average vertical velocity computed from heat flow and mass conservation remains remarkably constant, at around 43 mm/s (see Fig. 4(a)), supporting the fact that bubble size distribution doesn't change much as they move upward. The camera inspection video can also be used to put bounds on the bubble velocity, using a crude Particle Image Velocimetry technique: by cross-correlating successive video frames, an average displacement between the two can be obtained, which in turn depends on the average distance the bubbles traveled in the time between frames. Given the limited bubble loading and depth-of-field effects on the camera images, the distribution of velocities obtained through cross-correlation is fairly wide, but its peak, at 45.5 mm/s (see Fig. 4(b)), is very close to the value obtained from the measured bubble volume fraction and computed radial heat flow.

Unfortunately, correlating bubble velocity to shape and size is not easy: video inspection frames suggest an average diameter of 1.39 mm, with a standard deviation of 0.61 mm. Standard drag correlations would imply a very thin lenticular shape, with thickness equal to around 10% of radius; in reality the motion of an ascending bubble is fully three-dimensional and similar to a falling leaf, with

vortices shedding at the trailing edge and the shape affected by the motion itself. This makes trying to model bubble shape an extremely difficult task.

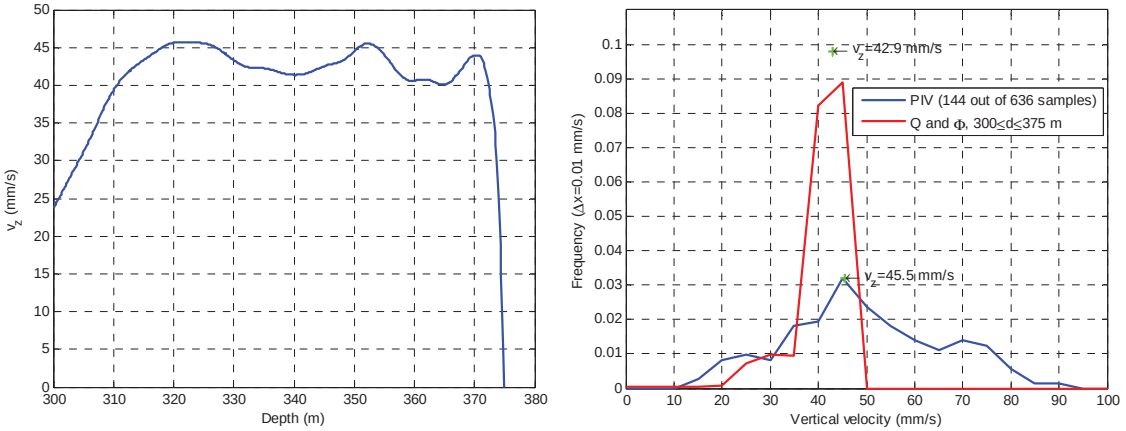

Fig. 4. (a) Vertical vapor CO_2 bubble velocity vs. depth computed from bubble volume fraction and predicted heat flow; (b) distribution of bubble vertical velocity from Particle Image Velocimetry (using camera inspection video frames) the profile plotted in (a).

5. The well as distillation column

The gas injected in Ketzin is >99.9% CO_2, with the rest mostly composed of nitrogen (N_2) and traces of non-condensable gases. During the reservoir transit, the gas most likely became saturated with water in equilibrium with reservoir brine, resulting in a mixture with around 0.09% water.

The presence of water has a huge effect on the thermodynamic behavior of CO_2, as shown in Fig. 5: the critical point moves far to the left, implying that the whole well should have been in dense phase at the time of the second wireline log. In reality at the time of CO_2 arrival, as the well started from the original conditions measured during the first log, the CO_2-water mixture (in vapor phase) would have bubbled to the air gap above the original top of brine at 96 m and would have pushed down the brine, at the same time increasing pressure to maintain hydrostatic balance at the formation. Following the green arrow in Fig. 5, the mixture would have hit the dew point curve, separating into a water-rich liquid phase and a CO_2-rich vapor phase.

Water would have collected at the top of brine, whereas vapor CO_2, with much reduced water content, would have accumulated in the (growing) air gap above the descending top of brine. As the pressure kept increasing, liquid CO_2 would condense and collect between the vapor phase and the brine free surface. The heat pipe evaporation-condensation that quickly established itself in the well would continue the distillation process, increasing CO_2 purity. A similar process would also purify CO_2 from any non-condensable gases, whether picked up in the reservoir or co-injected, which would then collect at the wellhead.

Since the heat pipe circulation can only take place to the left of the critical point, CO_2 purity could be expected to decrease with depth. This in fact appears to be the case: Fig. 2 shows that difference between measured density and the values predicted by [6] increases below 400 m, reaching a maximum of ~4% just below the critical point.

Distillation seems therefore to be the reason for the uncanny ability of the equation of state for pure CO_2 to describe the behavior of the fluid in Ktzi 200, even though the journey through the reservoir produced a complex and only partly known mixture.

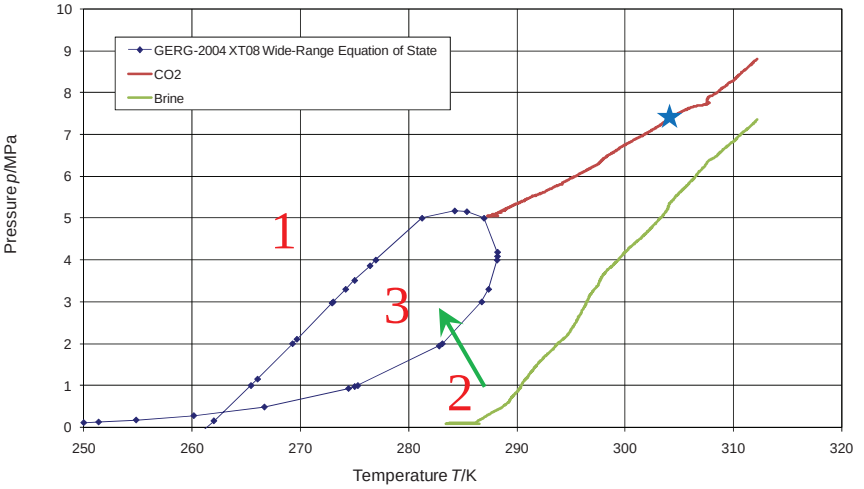

Fig. 5. Comparison of the phase diagram of a CO_2+0.085% H_2O mixture, representing injected CO_2 saturated with water at reservoir conditions and computed from the GERG-2004 equation of state, with the (p,T) curves of Ktzi 200 before (green) and after (red) CO_2 arrival. Above the upper branch of the blue curve (the bubble point curve) and to the left of the critical point, zone 1, the mixture is in liquid, whereas below the lower branch (the dew point curve), zone 2, the mixture is in vapor phase; between the two branches, in the zone 3, the mixture separates in a water-rich liquid phase and a CO_2-rich vapor phase. The blue star denotes the critical point of pure CO_2.

6. Summary and conclusions

The observation well Ktzi 200 has been producing a wealth of information about the unusual behavior of static, long columns of CO_2. Continuous temperature monitoring through an annular DTS fiber, coupled with frequent wireline logs and a camera inspection has allowed the identification of steady-state heat pipe circulation taking place above 400 m.

When wellhead pressure and temperature are below their critical values, a heat pipe is actually a very common feature of static wells full of CO_2, because of the temperature profile “capture” by the saturation line. When this happens, normal methods to rely surface to bottom-hole pressure fail and an alternative, iterative algorithm described in this paper should be used instead.

The iterative optimization algorithm finds the depth of the liquid CO_2 free surface that results in zero total heat flow in and out of the well. At each iteration, heat flow at each depth above the intersection of the CO_2 (p,T) curve with the saturation line is computed using a simple time-dependent 1-D model. The intersection of the two curves, i.e. the “capture depth”, can be found by integrating the mechanical equilibrium equation (Eq. 1) from the reservoir upward.

The success in predicting temperature and pressure profiles and the depth of the liquid CO_2 free surface in Ktzi 200 relies on the ability of the equation of state for pure CO_2 to model the behavior of the fluid in the well. A distillation process that operated at early times after CO_2 arrived at the well helps explain why this assumption is verified in practice.

Acknowledgements

The authors would like to thank the Ketzin project participants and all partners for their continued support and contributions. Research and operational work at the Ketzin pilot site is funded by the European Commission (Sixth and Seventh Framework Programs), the German Federal Ministry of Economics and Technology, the German Federal Ministry of Education and Research (GEOTECHNOLOGIEN Program) and industry partners.

Nomenclature

Δh_{ev}	enthalpy of evaporation, J/kg
Φ	volume fraction of bubbles, dimensionless
η	thermal conductivity, W/(m·K)
λ	viscosity, Pa/s
ρ	density, kg/m^3
A	specific surface area of casing, m^2/m
T	temperature, K or ºC
c_p	specific heat at constant pressure, J/(kg·K)
d	Measured Depth, i.e. the curvilinear abscissa of the well axis, m
g	acceleration of gravity, approximately equal to 9.81 m/s^2
p	pressure, MPa
q	heat flow, W/m
w	vertical velocity, m/s
z	Total Vertical Depth, i.e. depth measured along the vertical axis, pointing downward, m

References

[1] Martens S, Liebscher A, Möller F, Würdemann H, Schilling F, Kühn M, Ketzin Group. Progress Report on the First European on-shore CO_2Storage Site at Ketzin (Germany) - Second Year of Injection. *Energy Procedia* 2011; **4**: 3246-3253.

[2] Prevedel B, et al.. The CO2SINK boreholes for geological storage testing. *Scientific Drilling* 2008, **6**: 32-7.

[3] Zimmer M, Erzinger J, Kujawa C. The gas membrane sensor (GMS): A new method for gas measurements in deep boreholes applied at the CO2SINK site. *International Journal of Greenhouse Gas Control* 2011; **5**: 995-1001.

[4] Henninges J, Liebscher A, Bannach A, Brandt W, Hurter S, Köhler S, et al. P-T-rho and two-phase fluid condition with inverted density profile in observation wells at the CO_2 storage site at Ketzin (Germany), *Energy Procedia* 2011; **4**; 6085-6090.

[5] Paterson L, Lu M, Connell LD, Ennis-King J. Numerical modeling of pressure and temperature profiles including phase transitions in carbon dioxide wells, *SPE Annual Technical Conference and Exhibition* 2008; Denver (Colorado, USA).

[6] Span R, Wagner W. A New Equation of State for Carbon Dioxide Covering the Fluid Region from the Triple-Point Temperature to 1100 K at Pressures up to 800 MPa. *Journal of Physical and Chemical Reference Data* 1996;**25**:1509.